Reactive Power Dispatch Method in Wind Farms to Improve the Lifetime of Power Converter Considering Wake Effect

Tian, Jie; Zhou, Dao; Su, Chi; Chen, Zhe; Blaabjerg, Frede

Published in:
IEEE Transactions on Sustainable Energy

DOI (link to publication from Publisher):
10.1109/TSTE.2016.2607146

Publication date:
2017

Document Version
Accepted author manuscript, peer reviewed version

Reactive Power Dispatch Method in Wind Farms to Improve the Lifetime of Power Converter Considering Wake Effect

J. Tian, *Student member IEEE*, D. Zhou, *Member*, *IEEE* , C. Su, *Member*, *IEEE*, Z. Chen, *Senior member*, *IEEE* and F. Blaabjerg, *Fellow*, *IEEE*

***Abstract*—In Wind Farms (WF), the most popular and commonly implemented active power control method is the Maximum Power Point Tracking (MPPT). Due to the wake effect, the upstream Wind Turbine (WT) in WFs has more active power generation than the downstream WT at the wind directions and wind speeds that the WF has wake loss. In the case that WTs support the voltage control by reactive power, the upstream WT's power converter may have shorter lifetime even below the industrial standard. In this paper, based on the analysis of the wake effect, the reactive power capability of the Doubly Fed Induction Generator (DFIG) WT and the lifetime of DFIG WT's power converter, a reactive power dispatch method is proposed in the WF with DFIG WTs to improve the lifetime of the upstream WT's power converter. The proposed reactive power dispatch method is analyzed and demonstrated by the simulation on a WF with 80 DFIG WTs. It can be concluded that, compared with the traditional reactive power dispatch method, the proposed method can increase the lifetime of the upstream WT's power converter.**

***Index Terms*—lifetime, reactive power dispatch, voltage control, wake effect, wind farm.**

I. Nomenclature

u	Ambient wind speed
v	Downstream wind speed
C_t	Thrust coefficient
β	Pitch angle
λ	Tip-speed-ratio
D	Blade diameter
k	Decay constant
X	Position of the downstream wind turbine
$A_{overlap}$	Overlap area
A_R	Blade sweep area
P_s	Stator active power
Q_s	Stator reactive power
P_r	Rotor active power
Q_r	Rotor reactive power
P_{GSC}	Active power of the grid-side converter
Q_{GSC}	Ractive power of the grid-side converter
I_s	rms stator current
ω_s	Stator frequency
T_m	Mechanical torque
p	Number of pole pairs
V_s	rms stator voltage
φ_s	Stator power factor angle
P_m	Mechanical power
ω_m	Rotor mechanical angular speed
ω_r	Rotor electrical angular speed
R_s	Stator winding resistance
L_{ls}	Stator leakage inductance
L_m	Magnetizing inductance
L_s	Stator inductance
s	Slip
k_{sr}	Winding ratio between stator and rotor
σ	Leakage coefficient
R_r	Rotor winding resistance
L_{lr}	Rotor leakage inductance
L_r	Rotor inductance
V_r	rms rotor voltage
I_r	rms rotor current
φ_r	Rotor power factor angle
U_r	Converter voltage
P_T	IGBT loss
P_D	Diode loss
V_{ce}	Voltage drop during IGBT on-state
V_f	Voltage drop during diode on-state
E_{on}	Turn-on energy of IGBT
E_{off}	Turn-off energy of IGBT
E_{rr}	Reverse-recovery energy of diode
V_{dc}	Dc-link voltage of power converter
V_{dc}^*	Reference dc voltage during test
N	Carrier ratio
f_s	Switching frequency
f_e	Fundamental frequency of current
i_a	Current through each power component
T_s	Switching period
T_{jm_T}	Mean junction temperature of IGBT
dT_{j_T}	Junction temperature fluctuation of IGBT
T_{jm_D}	Mean junction temperature of diode
dT_{j_D}	Junction temperature fluctuation of diode
R_{thjc}	Thermal resistance from junction to case

This work was supported in part by the Sino-Danish Centre for Education and Research, Aarhus, DK-8000, Denmark.

J. Tian, D. Zhou, C. Su, Z. Chen and F. Blaabjerg are all with the Department of Energy Technology, Aalborg University, Aalborg, 9220, Denmark (e-mail: jti@et.aau.dk, zda@et.aau.dk, csu@et.aau.dk, zch@et.aau.dk, fbl@et.aau.dk).

R_{thca}	Thermal resistance from case to ambient
P	Power loss of each power semiconductor
T_a	Ambient temperature
t_{on}	On-state time within a fundamental period
t_e	Fundamental period of current
τ	Thermal time constant
AD	Annual damage
N_f	Cycle-to-failure of power semiconductor
β_1	Exponential coefficients of temperature swing
β_2	Exponential coefficients of mean temperature
β_3	Exponential coefficients of on-state time
β_4	Scaling factor of the lifetime model
$\overline{V_m}$	Magnetizing voltage (complex)
$\overline{V_s}$	Stator voltage (complex)
$\overline{I_s}$	Stator current (complex)
$\overline{I_m}$	Magnetizing current (complex)
$\overline{I_r}$	Rotor current (complex)
$\overline{V_r}$	Rotor voltage (complex)

II. Introduction

RENEWABLE energy is increasingly integrated into the modern power system. E.g., in Denmark, the wind power generation got 42.2% of its national electricity demand by the end of 2015, while the wind power target is 50% of the electricity demand by 2020 [1]. Consequently, wind farm (WF) supporting the voltage control has become an important issue. According to the grid codes [2] and [3], a WF must be equipped with the following three exclusive control functions: reactive power control, the power factor control and also the voltage control. Moreover, in [4] and [5], the authors proposed that WFs can also be employed to support the secondary voltage control, where the voltage reference at the Point of Common Coupling (PCC) or the reactive power reference of the WF is generated and sent out by the Automatic Voltage Control (AVC) in the power system.

Doubly fed induction generator (DFIG) based wind turbines (WT) have some amount of reactive power capabilities both from the stator side of the generator and from the Grid-Side Converter (GSC). Therefore, DFIG WT can be seen as continuous reactive power source. The reactive power capability of DFIG WT is analyzed in [6] and [7]. It depends on the active power generation of the WT, the voltage at the terminal of the WT and the current and voltage limit of the generator and the power converter. Other voltage control devices in WF include switching capacitor bank, taper-changer transformer, shunt reactor, static synchronous compensator (STATCOM) and static var compensator (SVC) etc. In [8] and [9], the authors proposed dispatch methods among different voltage control devices in WF in order to reduce the power loss on the connection cable and to reduce the operation cost of the discrete device e.g. the switching capacitor bank and the tap-changer transformer. Because of better economy and controllability, under the premise of providing sufficient voltage support, the DFIG WT has a higher priority to support the voltage control compared to other voltage control devices in the WF [8].

Recently, reliability issues in WT are becoming more and more of importance, especially when the WF moves from the onshore to the offshore. The harsh environment forces the WT system to operate up to 25 years due to the expensive offshore installation and maintenance. According to a field survey of WT system [10], the electrical part has the highest failure rated compared to other parts like the turbine, gearbox, generator and control. It can be inferred that the lifetime of the power converter is the shortest and determines the lifetime of WT system. Based on the thermal stress analysis of power electronics converter in [10], the lifetime of WT's power converter, defined as how many years it can continuously operate at the current working condition, depends on the WT's active power generation and reactive power generation, which are closely related to the WT's mission profile.

Wake effect in the WF is an important issue, especially in large-scale WFs. The obvious effect of the wake is the power loss of the WTs in a single wake or in multiple wakes. Many works have focused on the development of wake model [11] and [12]. With the consideration of the wake effect, WF layout optimization methods [13] and [14] and the active power control methods [15] and [16] have been developed for the power loss reduction. Because of the wake effect, downstream WT's available active power depends on the upstream WT's active power control method. Besides, there is interaction between the WF output power and the network. In [17], the authors presented the impact of the wake effect on the dynamic power system simulation. Furthermore, in [18], the authors presented the influence of the wake effect on the inertial response for the frequency control during the generation and load imbalance. In [19], the authors presented a coordinated control method for the WF to support the frequency control under the generation and load imbalance, considering the influence of the wake effect on the inertial response.

The popular and commonly implemented active power control method in WFs is the maximum power point tracking (MPPT) method for each WT to extract maximum active power from the wind. When the WTs are employed to provide extra reactive power to support the voltage control, the lifetime of WT's power converter could be reduced due to its additional current stress in each power module, which is an important challenge for modern WF lifetime requirement [10]. With the implemented MPPT method, due to the wake effect, upstream WT has more active power generation than downstream WT at the wind directions that the WF has wake loss [15], which results in shorter lifetime of upstream WT. Consequently, by using dispatching appropriate reactive power, (i.e. higher reactive power from the downstream WT, but lower reactive power from the upstream WT), the lifetime of each WT's power converter can be compromised, and the lifetime of upstream WT's power converter can be increased.

A reactive power dispatch method to balance the power

load among WTs is essentially to dispatch the reactive power requirement of each WT in the WF in proportion to its reactive power capability [20]. However, even with this method implemented, the lifetime of upstream WT's power converter could even be shorter than the industrial standard, while the downstream WTs could have very long lifetime. In this paper, an reactive power dispatch method is proposed to improve the lifetime of upstream WT's power converter, by trading-off the lifetime of each WT's power converter. Based on the reference of each WT's active power, the calculation of the lifetime of the each WT's power converter and the reactive power capability of each WT, the appropriate reactive power for each WT can be generated.

This paper is organized as follows. DFIG model and reactive power capability of DFIG WT are analyzed in Section III. The method to evaluate the lifetime of WT's power converter is introduced in Section IV. The proposed reactive power dispatch method to improve the lifetime of upstream WT's power converter is discussed in Section V. Simulation case studies on a WF with 80 NREL 5 MW DFIG WTs to analyze and demonstrate the proposed method is carried out in Section VI. Finally, some concluding remarks are drawn in Section VII.

III. DFIG Model and Reactive Power Capability

The typical configuration of DFIG WT is shown in Fig. 1. The reactive power from the stator side of the generator and the reactive power from the GSC can be generated by the DFIG WT and integrated into the power system.

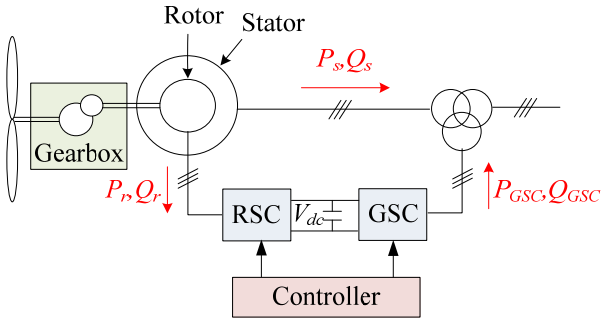

Fig. 1. Configuration of the DFIG WT.

A. DFIG Model

The steady-state equivalent circuit of a DFIG is shown in Fig. 2, where Z_{eq}/s is the equivalent impedance of the power converter. When the WT operates with a leading or lagging power factor, the stator current can be calculated by [21]

$$I_s = \frac{\omega_s T_m / p}{3V_s \cos\varphi_s} \tag{1}$$

where the mechanical torque can be calculated by,

$$T_m = \frac{P_m}{\omega_m} = \frac{P_m}{\omega_r / p} \tag{2}$$

The voltage across the magnetizing branch can be calculated by

$$\overline{V_m} = \overline{V_s} - \overline{I_s}(R_s + j\omega_s L_{ls}) \tag{3}$$

The magnetizing current can be calculated by,

$$\overline{I_m} = \frac{\overline{V_m}}{j\omega_s L_m} \tag{4}$$

The rotor current can be calculated by,

$$\overline{I_r} = \overline{I_s} - \overline{I_m} \tag{5}$$

The rotor voltage can be calculated by,

$$\overline{V_r} = s\overline{V_m} - \overline{I_r}(R_r + js\omega_s L_{lr}) \tag{6}$$

The slip s can be calculated by,

$$s = \frac{\omega_s - \omega_r}{\omega_s} \tag{7}$$

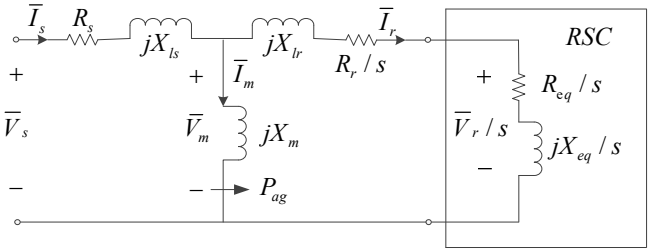

Fig. 2. Steady-state equivalent circuit of DFIG.

B. Reactive Power Capability of DFIG WT

Depending on the active power of the WT, the reactive power capability of DFIG WT which is limited by the stator current, the rotor current and the rotor voltage is analyzed in [6].

The reactive power from the stator side of the generator can be calculated by

$$Q_s = 3V_s I_s \sin\varphi_s \tag{8}$$

The maximum reactive power from the stator side of the generator limited by the stator current can be calculated by combining (1) and (8) at the maximum stator current. The maximum reactive power from the stator side of the generator limited by the rotor current can be calculated by combining (1)-(5) and (8) at the maximum rotor current. The maximum reactive power from the stator side of the generator limited by the rotor voltage can be calculated by combining (1)-(6) and (8) at the maximum rotor voltage.

The reactive power capability of the GSC, which depends on the active power from the rotor-side of the generator and the capability of the converter, can be calculated by

$$Q_{GSC} = \pm\sqrt{S_{GSC}{}^2 - P_r^2} \tag{9}$$

where the active power from the rotor-side of the generator can be calculated by

$$P_r = V_r I_r \cos\varphi_r \tag{10}$$

IV. Lifetime of Power Converter

The method to estimate the lifetime of the power electronics components in the WT system starts with mission profile inputs – the generated active power and required reactive power. With the help of the DFIG model and the loss model of the power electronics component, the loss dissipation of each IGBT and the diode can be calculated, both of which consist of conduction losses and switching losses. Based on a thermal model of the power module, the thermal profile of the power semiconductors can be calculated in terms of the mean junction temperature and the junction temperature fluctuation at the given active power and reactive power. They are closely related to the thermal resistance and thermal capacitance of the power module as well as its applied cooling solution. Afterwards, the B_{10} lifetime data can be obtained from the manufacturer at fixed thermal stress, and it can be further extended to the mean junction temperature and the junction temperature fluctuation at any freedom by using Coffin-Manson equation. Finally, the annual damage, which is defined as the annual cycles over the cycle-to-failure, can be calculated. If the mission profile is annually repeated, the lifetime expectancy of the power converter – reciprocal of the annual damage can be estimated.

By using this approach, the lifetime of the GSC and Rotor-Side Converter (RSC) can be estimated. Although the lifetime expectancy of the power converter is heavily dependent on its design criteria and its working environment (e.g. the power device selection, annual local wind speeds and wind conditions), a lifetime comparison between the GSC and RSC of a typical 2 MW DFIG is performed in [10], it is evident that the lifetime of the RSC is much lower compared to the GSC, which indicates that the lifetime of back-to-back power converter can simply be determined by the RSC.

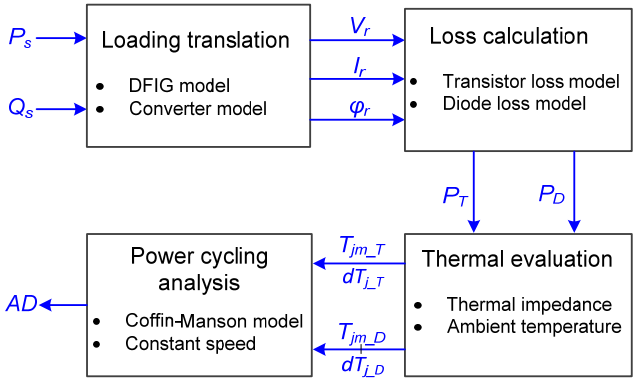

Fig. 3. Flowchart to estimate the lifetime of rotor-side converter at fixed active power and reactive power.

The detailed flowchart to estimate the lifetime of the RSC is shown in Fig. 3. Based on the requirement of the active power P_s and the reactive power Q_s, the procedure starts with the loading translation to calculate the rotor-side current $\overline{I_r}$ and voltage $\overline{V_r}$ of the DFIG [22],

$$\overline{I_r} = k_{sr}[-\frac{L_s}{L_m}\frac{P_s}{3V_s} + j(-\frac{V_s}{\omega_1 L_m} + \frac{L_s}{L_m}\frac{Q_s}{3V_s})] \tag{11}$$

$$\overline{V_r} = \frac{1}{k_{sr}}[s(\frac{L_r}{L_m}V_s - \frac{\sigma L_r L_s}{\omega_1 L_m}\frac{Q_s}{3V_s}) + j(-s\frac{\sigma L_r L_s}{\omega_1 L_m}\frac{P_s}{3V_s})] \tag{12}$$

where V_s denotes the stator voltage and ω_s denotes the stator frequency; L_m denotes the magnetizing inductance; L_s denotes the stator inductance – the sum of the stator leakage inductance L_{ls} and the magnetizing inductance, while L_r denotes the rotor stator inductance – the sum of the rotor leakage inductance L_{lr} and the magnetizing inductance; σ denotes leakage coefficient of the DFIG, defined as $(L_sL_r\text{-}L_m^2)/L_sL_r$; s denotes the slip value; and k_{sr} denotes the winding ratio between the stator and the rotor. Based on the complex terms of the rotor current and voltage, the displacement angle φ_r can be obtained.

The loss dissipation of the IGBT and the diode can be calculated according to the loss model of the power device, both of which consist of the conduction loss and the switching loss [23]. The loss dissipation of the IGBT P_T can be expressed as,

$$P_T = f_e \cdot \sum_{n=1}^{N}\{V_{ce}(|i_a(n)|)\cdot|i_a(n)|\cdot d(n)\cdot T_s + \frac{V_{dc}}{V_{dc}^*}[(E_{on}(|i_a(n)|) + E_{off}(|i_a(n)|)]\} \tag{13}$$

where the first term is the conduction loss, and the second term is the switching loss. V_{ce} is the voltage drop of the IGBT during its on-state period, E_{on} and E_{off} are the turn-on and the turn-off energy dissipated by the IGBT at a certain dc-link voltage V_{dc}^*, which are proportional to the actual dc-link voltage V_{dc}. All the information can be found in the manufacturer datasheet. Besides, d is the duty cycle for each switching pattern, which can be calculated by using the rotor voltage as well as its displacement angle in the case of the Space Vector Modulation (SVM) with a symmetrical modulation sequence method of the no-zero vector and zero-vector. N is the carrier ratio between the switching frequency f_s and the fundamental frequency f_e. i_a is the current through each power component, T_s is the switching period, and the subscript n is the n^{th} switching pattern.

Similarly, the loss dissipation of the diode P_D can be expressed as,

$$P_D = f_e \cdot \sum_{n=1}^{N}\{V_f(|i_a(n)|)\cdot|i_a(n)|\cdot[1-d(n)]\cdot T_s + \frac{V_{dc}}{V_{dc}^*}\cdot E_{rr}(|i_a(n)|)\} \tag{14}$$

The first term is the conduction loss, and the second term is the switching loss. V_f is the voltage drop during its on-state period, E_{rr} is the reverse-recovery energy dissipated by the diode, which is normally given by the manufacturer at a certain dc-link voltage. It can be seen that the IGBT and the diode conducts complementarily within a switching period. Moreover, the IGBT and the diode loss in (13) and (14) are aimed for the entire bridge. For each power semiconductor (the IGBT or the diode), the loss will only be a half.

Since the mean junction temperature T_{jm} and the junction temperature fluctuation dT_j are regarded as the two most important reliability indicators, they can be calculated as [23],

$$T_{jm\_T/D} = P \cdot \sum_{i=1}^{4} R_{thjc\_T/D(i)} + P \cdot \sum_{j=1}^{3} R_{thca\_(j)} + T_a \quad (15)$$

$$dT_{j\_T/D} = 2P \cdot \sum_{i=1}^{4} R_{thjc\_T/D(i)} \cdot \frac{[1-\exp(-t_{on}/\tau_{thjc\_T/D(i)})]^2}{1-\exp(-t_e/\tau_{thjc\_T/D(i)})} \quad (16)$$

In (15), R_{thjc} is the thermal resistance from the junction to case of the power module, R_{thca} is the thermal resistance of the cooling system, in which subscripts i and j denote four-layer and three-layer Foster structure for the power module and the cooling, respectively. P is the power loss of each power semiconductor, and T_a is the ambient temperature. In (16), t_{on} denotes the on-state time within each fundamental period of the current at the steady-state operation, t_e denotes the fundamental period of the current, τ denotes the thermal time constant of each Foster layer.

Based on the B_{10} lifetime model of the power semiconductor [23], [24], the cycle-to-failure of the IGBT and the diode N_f can be calculated,

$$N_f = \beta_4 \cdot dT_j^{\beta_1} \cdot \exp(\frac{\beta_2}{T_{jm}+273}) \cdot t_{on}^{\beta_3} \quad (17)$$

where β_1, β_2, and β_3 are exponential coefficients related to the temperature fluctuation, the mean temperature and the on-state time, respectively. β_4 denotes the scaling factor of the lifetime model.

The annual damage AD can be defined as ratio between the total thermal cycles per year and its related cycle-to-failure,

$$AD = \frac{365 \cdot 24 \cdot 3600 \cdot f_e}{N_f} \quad (18)$$

It is noted that the constant wind speed all over the year is assumed, and there is no downtime during the operational year. Besides, the wind direction is not taken into account as well. In the case of a real wind profile, the wind speed distribution can be considered by using Miner's rule [25], where the various thermal stresses have the same effect on wear-out degradation. As a result, the actual annual damage can be calculated considering the weighting factor of the individual wind speed. Meanwhile, due to the wake effect, although WTs in the WF cannot strictly follow the MPPT algorithm at the ambient wind speed, each of them essentially obeys the MPPT at its equivalent wind speed as aforementioned. As a result, the wind direction only affects the equivalent wind speed for each WT, and this factor can be considered as well.

Moreover, in the case of the reactive power compensation required from the DFIG system, since the injection from the stator side of the generator supported by the RSC is more effective and efficient compared to the GSC compensation [26], the reactive power injection from the stator side of the generator will only be focused on in the following.

V. Proposed Reactive Power Dispatch Method

Considering the active power difference among the WTs in the WF because of the wake effect, the proposed reactive power dispatch method aims to increase the lifetime of the upstream WT's power converter which is overly short, and moreover to maximize the total lifetime of the overall WT's power converters. The proposed reactive power dispatch method can be formulated by the objective function, the constraints and the control variables as described below.

The objective function:

$$Max(\sum_{i=1}^{n} \omega_{WT_i} L_{WT_i}(P_{WT_i}, Q_{WT_i})) \quad (19)$$

where n is the number of WTs in the WF. The lifetime of the the i^{th} WT's power converter L_{WTi}, which depends on the i^{th} WT's active power P_{WTi} and reactive power Q_{WTi}, can be obtained in lifetime look-up-table as discussed in Section IV. ω_{WTi} is the weight coefficient. When the lifetime of the WT's power converter is overly short, the weight coefficient is set to be a large value, and when the lifetime of the WT's power converter is overly long, the weight coefficient is set to be a small value, to make sure the lifetime of the WT's power converter, which is overly short, can be increased.

Following constraints are existing:

$$0 \le Q_{WTi} \le Q_{WTi\_cap} \quad (20)$$

$$\sum_{i=1}^{n} Q_{WTi} - Q_{loss} = Q_{WF} \quad (21)$$

$$V_{WT\_\min} \le V_{WTi} \le V_{WT\_\max} \quad (22)$$

where over-excited reactive power injection is assumed and the reactive power of the i^{th} WT Q_{WTi} is limited by the reactive power capability of the i^{th} WT Q_{WTi_cap}. Q_{WTi_cap} depends on the active power of each WT and the voltage at the terminal of the i^{th} WT as presented in Section III. The total reactive power of all the WTs plus the reactive power loss on the WF connection cable Q_{loss} should be equal to the reactive power reference of the WF Q_{WF}. V_{WTi} is the voltage at the terminal of WT_i. V_{WT_min} and V_{WT_max} are the down and up voltage limit at the terminal of the WT.

The reactive powers of each WT are the control variables. In this work, the reactive powers of each WT are generated with the Particle Swarm Optimization (PSO) based optimization algorithm [15]. The flow chart of the optimization algorithm is shown in Fig. 4. In the iterations of the optimization algorithm, the first step is to limit the reactive power of each WT by the constraints (20)-(22). In constraint (20), the reactive power capability of each WT depends on the active power of each WT and the voltage at the terminal of each WT. The voltage at the terminal of each WT and the power loss on the connection cable can be obtained by the WF power flow calculation, with the active power of each WT, the voltage at PCC and the reactive power of each WT. Finally, the reactive power of each WT can be obtained by the lifetime

calculation and comparison of the objective function (19).

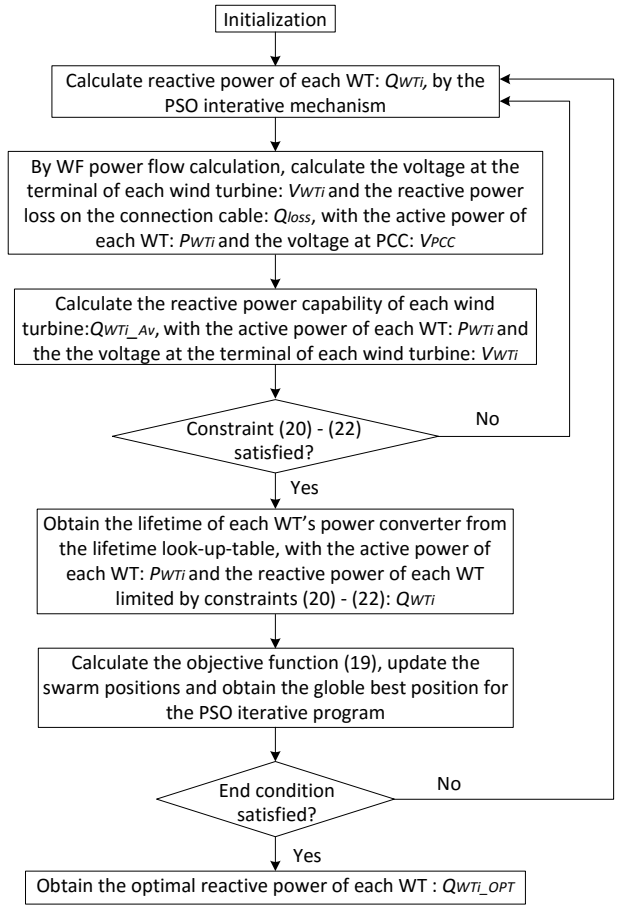

Fig. 4. Flow chart to obtain the reactive power for each WT, with the PSO based optimization algorithm.

VI. Case Study and Discussion

In this section, the proposed reactive power dispatch method is analyzed and demonstrated in a WF with 80 NREL 5 MW DFIG WTs. The layout of the WF, which is the same with the offshore WF of Horns Rev 1 in Denmark, is shown in Fig. 5. The distance between two adjacent WTs in the same row or in the same column is 819 m, which is 6.5 times of the blade diameter. The parameters of the NREL 5MW WT are enclosed in the appendix Table I.

A. Active Power Generation

To estimate the active power generation of each WT in the WF, the active power curve as shown in Fig. 6 [27] is assumed to be implemented in the WT control system. The active power curve incorporates 5 control regions, where the MPPT is implemented in region 3. The active power of each WT is estimated by the Katic model [28] and [15]. The WF is assumed to be an offshore WF and the decay constant k=0.04 is adopted [29].

The highest power losses of the WF, because of the wake effect, appears at the wind directions that are aligned to the symmetry axes of the WF [11]. In this case study, the high power loss appears at the wind directions of around 41°, 90°,

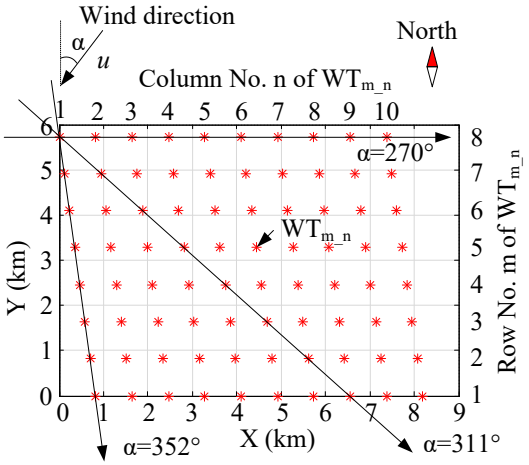

Fig. 5. Layout of the WF with 80 NREL 5 MW WTs.

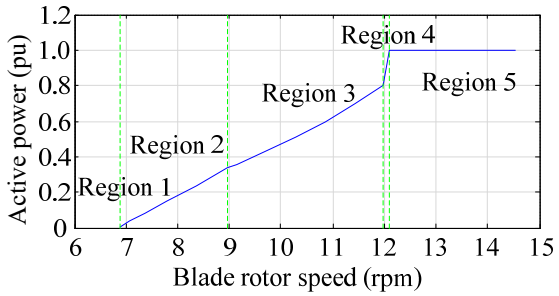

Fig. 6. Active power curve of the NREL 5 MW WT.

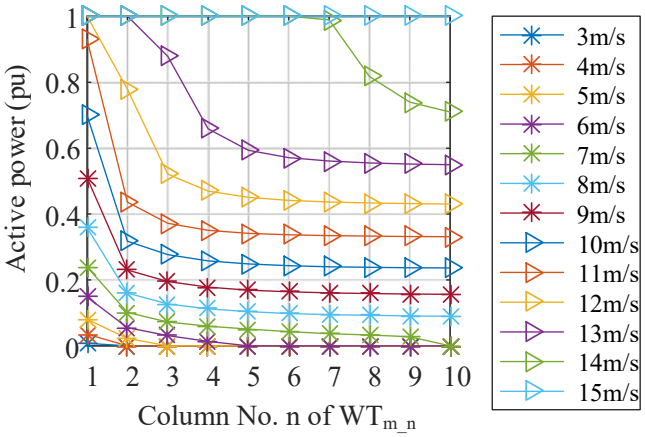

Fig. 7. Active power of the WTs in each column at 270° wind direction and at the wind speeds from 3 m/s to 15 m/s with the resolution of 1 m/s.

131°, 172°, 221°, 270°, 311° and 352°. At these wind directions the WTs have the most different active power generation. In order to illustrate the difference of each WT's active power generation, the active power generations of each WT at 270° wind direction and at the wind speeds in the range of 3 m/s to 15 m/s are calculated and shown in Fig. 7. At this wind direction, WTs in the same row will not cause the wind speed deficit for WTs in other rows. Thus, the WTs in the same column (as shown in Fig. 5, WT$_{m_n}$ is marked with its row No. m and column No. n) have the same active power generation.

B. Reactive Power Capability

As analyzed in [6], the over-excited reactive power capability of the DFIG WT is limited by the maximum rotor current. At stator voltages of 0.9 pu, 1.0 pu and 1.1 pu, the maximum reactive power from the stator side of the generator in terms of active power generation are shown in Fig. 8. To make sure that the WT is able to generate the rated active power at the stator voltages in the range of 0.9 pu to 1.1 pu, the maximum rotor current is selected to be 1.11 pu. It should be noticed that, in this case study, the rated power and the rated stator phase voltage have been used as the base value for the normalization.

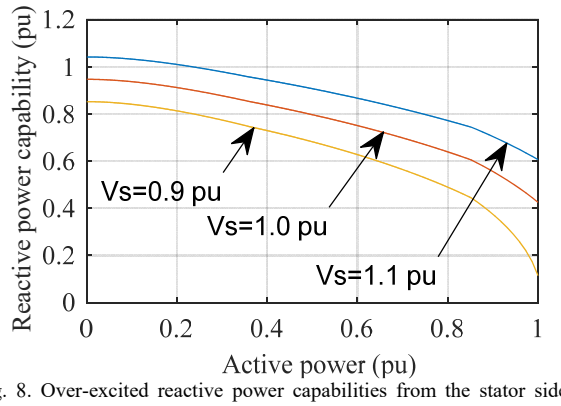

Fig. 8. Over-excited reactive power capabilities from the stator side of the generator in terms of the WT active power, at stator voltages of 0.9 pu, 1.0 pu and 1.1 pu.

At 270° wind direction, according to each WT's active power as shown in Fig. 7 and the WT's over-excited reactive power capability from the stator side of the generator as shown in Fig. 8, each WT's over-excited reactive power capabilities from the stator side of the generator at the ambient wind speeds in the range of 3 m/s to 15 m/s are shown in Fig. 9, where the stator voltage is assumed to be 1.0 pu.

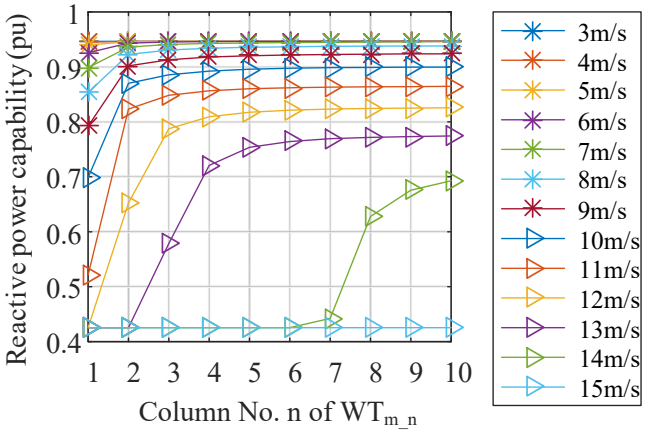

Fig. 9. Reactive power capability of the WT in each column, at 270° wind direction and at the wind speeds from 3 m/s to 15 m/s with the resolution of 1 m/s.

C. Lifetime of the Power Converter

In the DFIG system, although the active power flowing through the RSC is exactly the same as the GSC, the thermal loading of the RSC is much higher than the GSC [10]. Not only the RSC is normally required to excite the rotor-side of the generator in order to guarantee the unity power factor operation at the stator side of the generator, but also the rotor voltage is much lower than the grid voltage, which results in the higher current stress of the RSC. Besides, the operation frequency of the RSC is also much lower than the GSC, which causes high thermal cycling. As stated in Section IV, the lifetime of the power converters is typically decided by the RSC. Moreover, the reactive power compensation from the RSC further affects its reliability. As the under-excited reactive power relieves the stress of the RSC, while the over-excited reactive power imposes its thermal stress [25], only the over-excited reactive power is concerned.

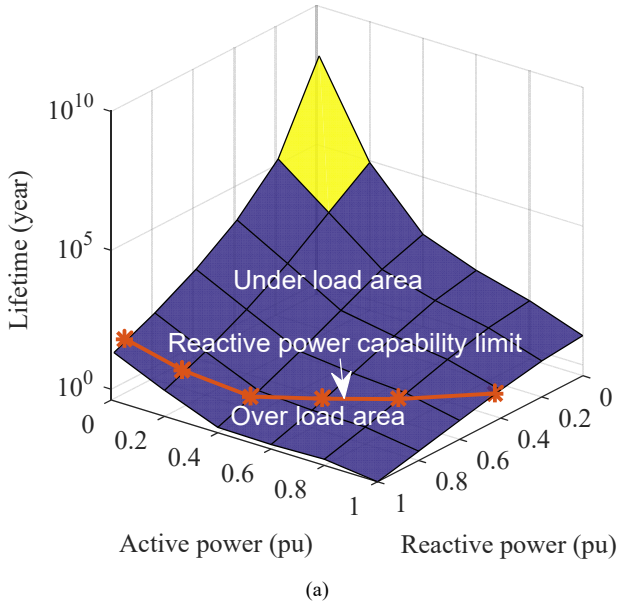

(a)

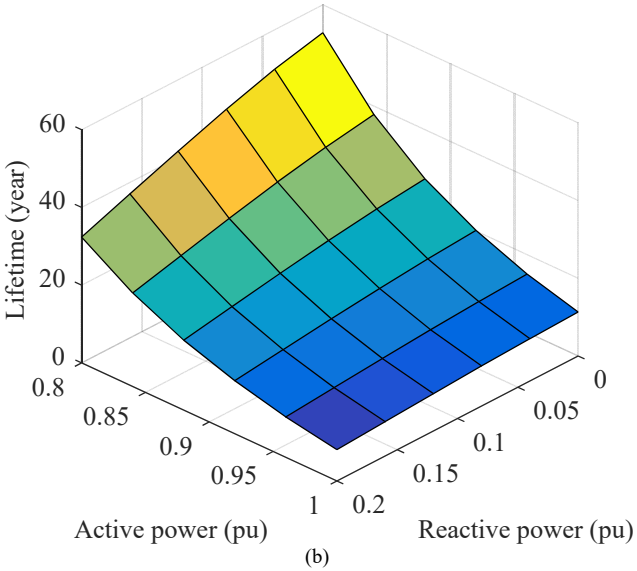

(b)

Fig. 10. Lifetime of the DFIG WT's power converter in terms of active power and reactive power. (a) Active power from 0 pu to 1 pu and the reactive power from 0 pu to 1 pu. (b) Active power from 0.8 pu to 1 pu and the reactive power from 0 pu to 0.2 pu.

According to the parameters of the DFIG listed in Table I

as well as the reliability data of power device listed in Table II, the lifetime of the power converter is shown in Fig. 10 in terms of various amounts of active power and reactive power. It is noted that, if the reactive power keeps constant, the lifetime is decreasing with higher active power except for the area around the active power of 0.4 pu. It is because the DFIG operates at the synchronous operation, and the low operation frequency results in relatively high thermal stress in spite of the low generated active power. Moreover, in the condition of the same amount active power, the higher reactive power causes a lower lifetime due to its higher thermal stress induced by the additional reactive power. Furthermore, the huge difference of lifetime can be found between the light load (with no active power and reactive power injection) and the heavy load (with 1.0 pu active power and reactive power injection). Assuming that no reactive power is required and 1.0 pu active power is provided all the year around, the lifetime of the RSC is 11.4 years.

D. Reactive Power Dispatch

Compared with the reactive power control method that dispatches the reactive power requirement of each WT in the WF in proportion to its reactive power capability, the optimization results obtained by the optimization algorithm are shown in Fig. 11, at the 270° wind direction, at the 12 m/s wind speed, at the 1.0 pu voltage at PCC and at the 0.44 pu, 0.50 pu and 0.63 pu reactive power of the WF. The weight coefficient in the objective function (19) is set to be $(11.4/L_{WTi})^3$, where 11.4 is the lifetime of the WT's power converter when the WT is working at the rated power and no reactive power output.

The optimized reactive power for each WT is shown in Fig. 11 (a). The lifetime of each WT's power converter with the optimized reactive power for each WT is shown in Fig. 11 (b). In Fig. 11 (b), it can be seen that the lifetime of the WT's power converter in column 1 is increased from 8.1 years, 7.6 years and 6.5 years to 11.3 years respectively, at the 0.44 pu, 0.50 pu and 0.63 pu reactive power of the WF. And the total lifetime of all the 80 WT's power converter is increased from 31976 years, 24544 years and 11088 years to 37384 years, 26000 years and 11600 years respectively, at the 0.44 pu, 0.50 pu and 0.63 pu reactive power of the WF.

E. Annual Lifetime Consumption

The effectiveness of the proposed reactive power dispatch method depends on the wind direction and wind speed distribution at the WF location area and the WF layout. The reasons are as follows.

- Only at the wind directions that the WF has wake loss, WTs have different active power generations and the proposed method can improve the lifetime of the upstream WT's power converter.
- As shown in Fig. 10, at low active power and low reactive power, the WT's power converter has very long lifetime, and therefore the power converter's lifetime consumption can be neglected.

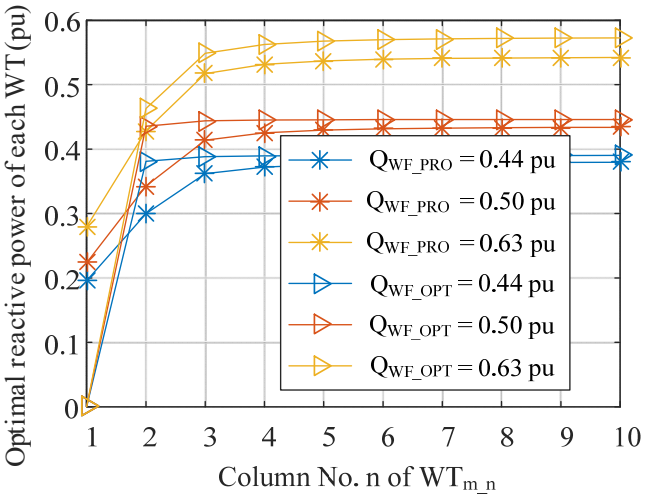

(a)

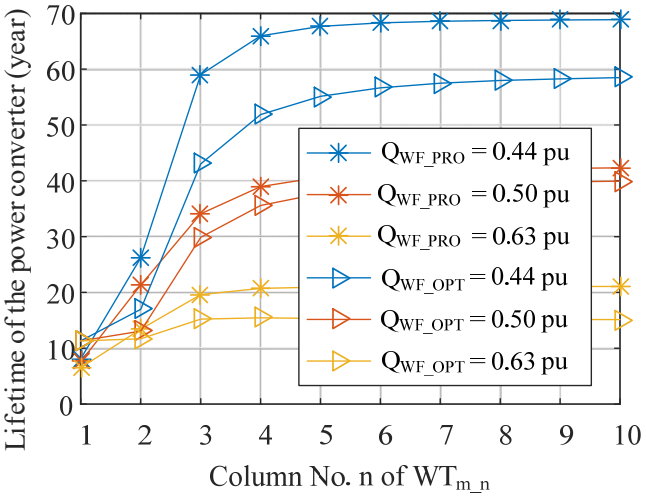

(b)

Fig. 11. Comparison between the proposed reactive power dispatch method and the method that dispatches the total reactive power for all WTs to each WT in proportion to the reactive power capability of each WT. (a) Reactive power of the WT in each column; (b) Lifetime of the WT's power converter of the WT in each column.

- The lifetime of the upstream WT's power converter is increased by sacrificing the lifetime of downstream WT's power converter. At opposite wind directions, upstream WT and downstream WT will be transferred to be the downstream WT and upstream WT. Thus, the effect of the proposed method will be weakened.

The lifetime of the power converter as shown in Fig. 10 is obtained by the assumption of the constant active and reactive power injection all the year around. Taking into account the factors of wind speed and wind direction distribution, the annual lifetime consumption defined as the percentage of lifetime consumed in one year is used in this paper to demonstrate the proposed reactive power dispatch method. The annual wind direction and wind speed data as shown in Fig. 12 are adopted to calculate the annual lifetime consumption of each WT's power converter. The wind direction distribution and the wind speed distribution as

shown in Fig. 13 are generated by the WAsP climate analysis tool with the data as shown in Fig. 12. The wind rose is separated into 36 sectors each with 10°.

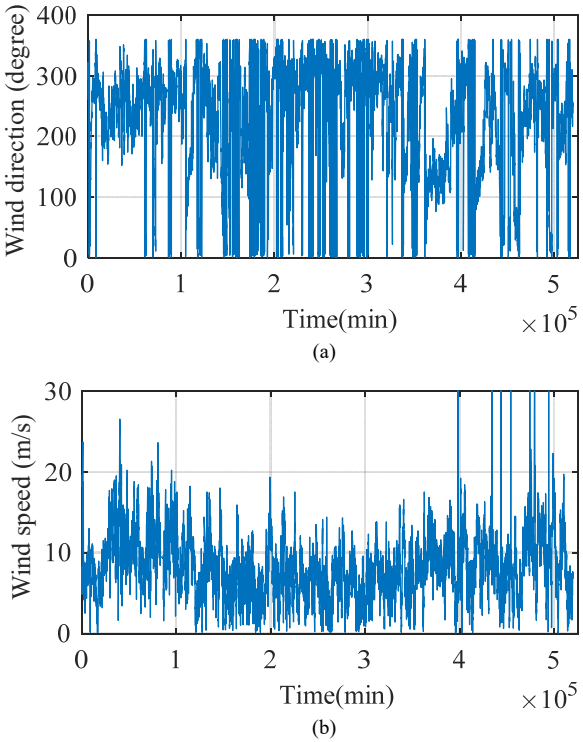

Fig. 12. (a) Annual wind direction time series; (b) Annual wind speed time series.

With the active power curve as shown in Fig. 6 implemented and compared between the proposed reactive power dispatch method and the method that dispatches the total reactive power for all WTs to each WT in proportion to each WT's reactive power capability, the annual lifetime consumption of each WT's power converter is shown in Fig. 14, where WT_{m_n} as shown in Fig. 5 are represented by $WT_{(m-1)\times 10+n}$. It can be seen that, the annual lifetime consumption of the WTs in column 1 can be reduced by the proposed method. When the WTs provide the total reactive power injection of 0.5 and 0.8 times the total reactive power capability of all the WTs, the annual lifetime consumption of the WT_{1_1}'s power converter is reduced by 5.01% and 7.15%, respectively.

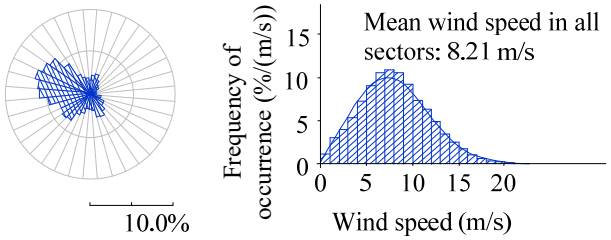

Fig. 13. Wind direction distribution in each wind rose sectors and wind speed distribution in all the wind rose sectors.

VII. Conclusions

The lifetime of the WT's power converter depends on the WT's active power and reactive power mission profile. Considering the wake effect, the WTs in a WF have different active power generations. By dispatching the reactive power among WTs, the lifetime of upstream WT's power converter, which has shorter lifetime even than the industrial standard, can be increased by sacrificing the lifetime of downstream WT's power converter which has much longer lifetime.

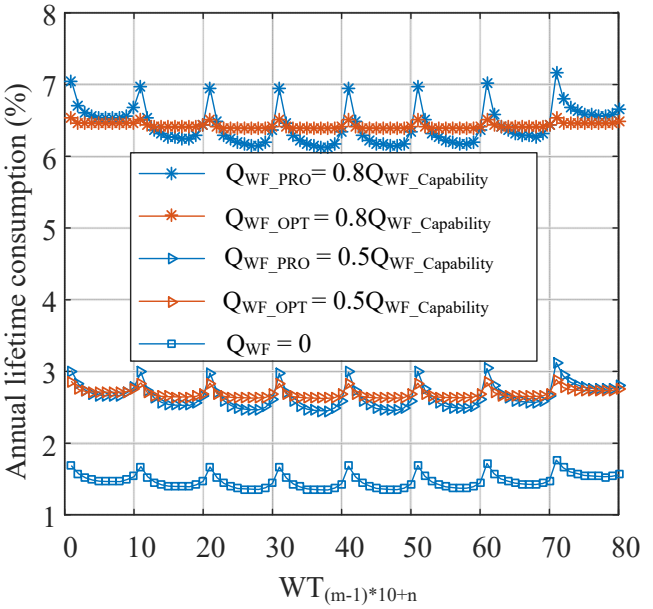

Fig. 14. Comparison of the annual lifetime consumption of each WT's power converter between the proposed reactive power dispatch method and the method that dispatches the reactive power reference for the WF to each WT in proportion to each WT's reactive power capability.

In this paper, an reactive power dispatch method among DFIG WTs in a WF is proposed to increase the lifetime of upstream WT's power converter which is overly short and to increase the total lifetime of all the WT's power converters. The proposed method generates the reactive power for each WT by the PSO based optimization algorithm based on the difference of each WT's active power generation because of wake effect and the reactive power for each WT is limited by each WT's reactive power capability.

At the wind directions where there is no wake loss in the WF and at high wind speeds that each WT are operating at the rated power, the active power generations of each WT are all the same. On the other side, at the lower wind speeds and lower reactive power requirements for the WF, the lifetime consumption of the WT's power converter can be neglected. Additionally, the trade-off for the lifetime between the upstream WT's power converter and downstream WT's power converter will be weakened at opposite wind directions. Thus, the effectiveness of the proposed method depends on the wind direction and wind speed distribution and the layout of the WF.

It can be concluded that, compared with the traditional reactive power dispatch method, the proposed method can increase the lifetime of the upstream WT's power converter and the total lifetime of all the WT's power converters. Moreover, the proposed method can be used for any WF

layout and at any wind direction and wind speed distribution at the WF area.

VIII. Appendix

TABLE I
Parameters of the 5 MW DFIG WT

WT		
Rated Mechanical Power	5 MW	
Rotor Diameter	126 m	
Hub Height	90 m	
Cut-In, Rated, Cut-Out Wind Speed	3 m/s, 11.4 m/s, 25 m/s	
Cut-In, Rated Rotor Speed	6.9 rpm, 12.1 rpm	
Gearbox ratio	97	
DFIG		
Rated Mechanical Power	5.0 MW	1.0 pu
Rated Stator Phase Voltage	548 V (rms)	1.0 pu
Rated Rotor Phase Voltage	381 V (rms)	0.6947 pu
Rated Stator Current	2578 A (rms)	0.8485 pu
Rated Rotor Current	3188 A (rms)	1.0494 pu
Rated Stator Frequency	50 Hz	1.0 pu
Number of Pole Pairs	3	
Stator Winding Resistance	1.552 mΩ	0.0086 pu
Rotor Winding Resistance	1.446 mΩ	0.008 pu
Stator Leakage Inductance	1.2721 mH	2.2141 pu
Rotor Leakage Inductance	1.1194 mH	1.9483 pu
Magnetizing Inductance	5.5182 mH	9.6044 pu
Power converter		
DC-link voltage	1600 V	1.684pu
Switching frequency	2 kHz	

TABLE II
Parameters used in loss model and thermal model of power semiconductors

		IGBT	Diode
Loss model	V_{ce} @ 1 kA, T_j=150 ºC (V)	2.45	/
	V_f @ 1 kA, T_j=150 ºC (V)	/	1.95
	E_{on} @ 1 kA, T_j=150 ºC (mJ)	430	/
	E_{off} @ 1 kA, T_j=150 ºC (mJ)	330	/
	E_{rr} @ 1 kA, T_j=150 ºC (mJ)	/	245
Thermal model	Fourth order thermal resistance (ºC/kW)	0.3	0.48
		1.6	3.61
		18	34.6
		3.1	6.47
	Four order thermal time constant (s)	0.003	0.0002
		0.0013	0.0009
		0.04	0.03
		0.4	0.2

IX. References

[1] IEA, 2014 IEA wind annual report (August 2015). [Online]. Available: http://www.ieawind.org.

[2] Energinet, "Technical Regulation 3.2.5. for Wind Power Plants with a Power Output Greater than 11 kW," Energinet, Fredericia, DK, 2010.

[3] M. Mohseni, and S. M. Islam, "Review of international grid codes for wind power integration: diversity, technology and a case for global standard," *Renewable and Sustainable Energy Reviews*, vol. 16, no. 6, pp. 3876–3890, Aug. 2012.

[4] M. S. El-Moursi, G. Joos, and C. Abbey, "A secondary voltage control strategy for transmission level interconnection of wind generation," *IEEE Trans. Power Electronics*, vol. 23, no. 3, pp. 1178–1190, May, 2008.

[5] N. Qin, H. Abildgaard, P.Lund, E. Dmitrova, T. Lund, P. B. Eriksen, C. L. Bak, and Z.Chen, "Automatic Voltage Control (AVC) of Danish Transmission System-Concept design," presented at the CIGRE US National Committee, 2014 Grid of the Future Symposium.

[6] J. Tian, C. Su, and Z. Chen, "Reactive Power Capability of the Wind Turbine with Doubly Fed Induction Generator," in *Proc. 2013 39th IEEE Industrial Electronics Society Conf.,* pp. 5310–5315.

[7] T. Lund, P. Sorensen, and J. Eek, "Reactive power capability of a wind turbine with doubly fed induction generator," *Wind Energy*, vol. 10, pp. 379–394, Apr. 2007.

[8] H. F. Chen, Y. Qiao, and Z. X. Lu, "Study on coordinated voltage control strategy of DFIG wind farm," in *Proc. 2012 IEEE PES General Meeting Conf.,* pp. 1–9.

[9] I. Erlich, W. Nakawiro, and M. Martinez, "Optimal dispatch of reactive sources in wind farms," in *Proc. 2011 IEEE PES Conf*., pp. 1–7.

[10] D. Zhou, F. Blaabjerg, M. Lau, and M. Tonnes, "Optimized reactive power flow of DFIG power converters for better reliability performance considering grid codes," *IEEE Trans. Industrial Electronics,* vol. 62, no. 3, pp. 1552–1562, Mar. 2015.

[11] R. J. Barthelmie, K. Hansen, S. T. Frandsen, O. Rathmann, J. G. Schepers, W. Schlez, J. Phillips, K. Rados, A. Zervos, E. S. Politis, and P. K. Chaviaropoulos, "Modelling and measuring flow and wind turbine wakes in large wind farms offshore," *Wind Energy*, vol. 12, no. 5, pp. 431–444, 2009.

[12] A. Duckworth, and R. J. Barthelmie, "Investigation and validation of wind turbine wake models," *Wind Engineering*, vol. 32, no. 5, pp. 459–475, 2008.

[13] A. Kusiak and Z. Song, "Design of wind farm layout for maximum wind energy capture," *Renew. Energy*, vol. 35, no. 3, pp. 685–694, 2010.

[14] S. Chowdhury, J. Zhang, A. Messac, and L. Castillo, "Unrestricted wind farm layout optimization (UWFLO): Investigating key factors in fl uencing the maximum power generation," *Renew. Energy*, vol. 38, no. 1, pp. 16–30, 2012.

[15] J. Tian, C. Su, M. Soltani, and Z. Chen, "Active power dispatch method for a wind farm central controller considering wake effect, " in *Proc. 2014 40th IEEE Industrial Electronics Society Conf.,* pp. 5450–5456.

[16] J. Serrano González, M. Burgos Payán, J. Riquelme Santos, and Á. G. González Rodríguez, "Maximizing the overall production of wind farms by setting the individual operating point of wind turbines," *Renew. Energy*, vol. 80, pp. 219–229, 2015.

[17] F. Koch, M. Gresch, F. Shewarega, I. Erlich, and U. Bachmann, "Consideration of Wind Farm Wake Effect in Power System Dynamic Simulation," *Power Tech, 2005 IEEE Russia*, vol. 2, no. 3, pp. 1–7.

[18] S. Kuenzel, S. Member, L. P. Kunjumuhammed, B. C. Pal, I. Erlich, and S. Member, "Impact of Wakes on Wind Farm Inertial Response," *IEEE Trans. Sustainable Energy,* vol. 5, no. 1, pp. 237–245, 2014.

[19] C. Kim, Y. Gui, and C. C. Chung, "Coordinated Wind Power Plant Control for Frequency Support under Wake Effects," in *Proc. 2015 IEE Power & Energy Society Meeting,* pp. 1–5, 2015.

[20] D. Hansen, P. Sorensen, F. Iov, and F. Blaabjerg, "Centralised power control of wind farm with doubly fed induction generators," *Renewable Energy*, vol. 31, no. 7, pp. 935–951, Jun. 2006.

[21] B. Wu, Y. Lang, N. zargari, and S. Kouro, *Power Conversion and Control of Wind Energy Systems*. New jersey: Wiley, 2011, pp. 254, 241–242.

[22] G. Abad, J. Lopez, M. Rodriguez, L. Marroy, and G. Iwanski. *Doubly Fed Induction Machine: Modeling and Control for Wind Energy Generation Applications*. Wiley-IEEE Press, 2011.

[23] D. Zhou, F. Blaabjerg, T. Franke, M. Tonnes, and M. Lau, "Comparison of wind power converter reliability with low-speed and medium-speed permanent-magnet synchronous generators," *IEEE Trans. Industrial Electronics*, vol. 62, no. 10, pp. 6575–6584, Oct. 2015.

[24] R. Amro, J. Lutz, and A. Lindemann, "Power cycling with high temperature swing of discrete components based on different technologies," *in Proc, of PESC 2004*, pp. 2593-2598, 2004.

[25] H. C. Yildirim, G. Marquis, and Z. Barsoum, " Fatigue assessment of high frequency mechanical impact (HFMI)-improved fillet welds by local approaches," *International Journal of Fatigue*, vol. 52, pp. 57–67, 2013.

[26] D. Zhou, F. Blaabjerg, M. Lau, and M. Tonnes, "Reactive power impact on lifetime prediction of two-level wind power converter," *in Proc. of PCIM 2013*, pp. 564–571, 2013.

[27] J. Jonkman, S. Butterfield, W. Musial, and G. Scott, "Definition of a 5-MW Reference Wind Turbine for Offshore System Development," Golden, CO: National Renewable Energy Laboratory, Tech. Rep. NREL/TP-500-38060, Feb. 2009.

[28] I. Katic, D. Højstrup, and N. O. Jensen, "A sample model for cluster efficiency," in *Proc. 1986 European Wind Energy Association Conf.*, pp. 407–410.

[29] N. G. Mortensen, D. N. Heathfield, L. Myllerup, L. Landberg and O. Rathmann, Wind Atlas Analysis and Application Program: WAsP 8 Help Facility. Risø National Laboratory, Roskilde, DK. 335 topics. ISBN 87-550-3457-8, 2005.

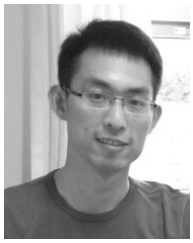

Jie Tian (S'2013) received the B.Eng. and M.Sc. degrees from Yanshan University, China, in 2005 and 2011 respectively. He is now a Ph.D. Student with the Department of Energy Technology, Aalborg University, Aalborg, Denmark. He is working on the advanced coordinative control of the wind power conversion system.

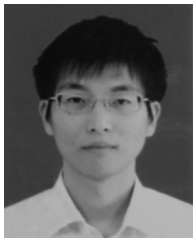

Dao Zhou (S'12, M'15) received the B.S. in electrical engineering from Beijing Jiaotong University, Beijing, China, in 2007, the M.S. in power electronics from Zhejiang University, Hangzhou, China, in 2010, and the Ph.D. from Aalborg University, Aalborg, Denmark, in 2014.

He is currently a Postdoctoral Researcher in Aalborg University. His research interests include power electronics and reliability in renewable energy application.

Dr. Zhou received the Renewable and Sustainable Energy Conversion Systems of the IEEE Industry Applications Society First Prize Paper Award in 2015, and Best Session Paper at Annual Conference of the IEEE Industrial Electronics Society (IECON) in Austria in 2013. He serves as a Session Chair for various technical conferences.

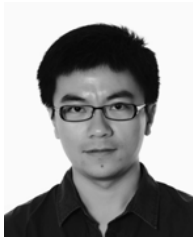

Chi Su (S'11–M'13) received the B.Eng. and M.Sc. degrees from Huazhong University of Science and Technology (HUST), China, in 2003 and 2007 respectively, and Ph.D. degree from Aalborg University, Denmark, in 2012. He is now working at the Department of Energy Technology, Aalborg University as an Assistant Professor. His research interests include power system oscillation and its wide-area control, wind power integration, protection and communication in distribution systems, and application of artificial intelligence in power system.

Zhe Chen (M'95–SM'98) received the B.Eng. and M.Sc. degrees from Northeast China Institute of Electric Power Engineering, Jilin, China, and the Ph.D. degree from the University of Durham, Durham, U.K.

He is currently a Full Professor with the Department of Energy Technology, Aalborg University, Aalborg, Denmark, where he is the Leader of the Wind Power System Research Program. He is the Danish Principal Investigator for Wind Energy of the Sino-Danish Centre for Education and Research. He has authored or coauthored more than 320 publications in his technical field. His current research interests include power systems, power electronics, electric machines, wind energy, and modern power systems.

Dr. Chen is a Fellow of the Institution of Engineering and Technology, U.K., and a Chartered Engineer in the U.K. He is an Associate Editor (Renewable Energy) of the IEEE TRANSACTIONS ON POWER ELECTRONICS.

Frede Blaabjerg (S'86–M'88–SM'97–F'03) was with ABB-Scandia, Randers, Denmark, from 1987 to 1988. From 1988 to 1992, he was a Ph.D. Student with Aalborg University, Aalborg, Denmark. He became an Assistant Professor in 1992, Associate Professor in 1996, and Full Professor of power electronics and drives in 1998. His current research interests include power electronics and its applications such as in wind turbines, PV systems, reliability, harmonics and adjustable speed drives.

He has received 17 IEEE Prize Paper Awards, the IEEE PELS Distinguished Service Award in 2009, the EPE-PEMC Council Award in 2010, the IEEE William E. Newell Power Electronics Award 2014 and the Villum Kann Rasmussen Research Award 2014. He was an Editor-in-Chief of the IEEE TRANSACTIONS ON POWER ELECTRONICS from 2006 to 2012. He is nominated in 2014 and 2015 by Thomson Reuters to be between the most 250 cited researchers in Engineering in the world.